2012

Effect of partial preferential orientation and distortions in octahedral clusters on the photoluminescence properties of FeWO4 nanocrystals

CRYSTENGCOMM, CAMBRIDGE, v. 14, n. 21, supl. 1, Part 3, pp. 7127-7132, APR 30, 2012
http://www.producao.usp.br/handle/BDPI/40820

CrystEngComm

Cite this: *CrystEngComm*, 2012, **14**, 7127–7132

www.rsc.org/crystengcomm

COMMUNICATION

Effect of partial preferential orientation and distortions in octahedral clusters on the photoluminescence properties of $FeWO_4$ nanocrystals†

M. A. P. Almeida,[a] L. S. Cavalcante,*[b] C. Morilla-Santos,[c] C. J. Dalmaschio,[a] S. Rajagopal,[e] M. Siu Li[d] and E. Longo[ab]

Received 17th May 2012, Accepted 2nd August 2012
DOI: 10.1039/c2ce25771h

This communication is a report of our initial research to obtain iron tungstate ($FeWO_4$) nanocrystals by the microwave-hydrothermal method at 170 °C for 45 min. X-ray diffraction patterns showed that the $FeWO_4$ nanocrystals prepared with polyethylene glycol-200 have a partial preferential orientation in the (011) plane in relation to other nanocrystals prepared with sodium bis(2-ethylhexyl)sulfosuccinate and water. Rietveld refinement data indicates that all nanocrystals are monophasic with wolframite-type monoclinic structures and exhibit different distortions on octahedral [FeO_6]/[WO_6] clusters. High resolution transmission electron microcopy revealed an oriented attachment mechanism for the growth of aggregated $FeWO_4$ nanocrystals. Finally, we observed that the photoluminescence properties of these nanocrystals are affected by partial preferential orientation in the (011) plane and distortions on [FeO_6]/[WO_6] clusters.

1. Introduction

In recent years, much research has been devoted to the synthesis of new nanomaterials with good physical/chemical properties in relation to bulk materials.[1–3] Metal tungstates with a general formula (MWO_4) represent an important group of inorganic oxides with excellent functional and electronic properties.[4–6] Their crystalline structure can be composed of M-bivalent cations with large radii (M = Ca, Sr, Ba, Pb) and small radii (M = Fe, Mn, Co, Zn). These tungstates exhibit differences in the coordination of their clusters. The first tungstate oxides have a scheelite-type tetragonal structure where cations with large radii are linked to eight oxygen atoms which form [MO_8] clusters with deltahedral coordination, while W atoms are bonded to four oxygen atoms which results in the formation of tetrahedral [WO_4] clusters.[7,8] The second tungstate oxides exhibit a wolframite-type monoclinic structure where both M and W atoms are bonded to six oxygen atoms, which results in the formation of octahedral [MO_6]/[WO_6] clusters.[9,10] These differences in the coordination/structure cause defects in the crystal lattice and the appearance of photocatalytic,[11,12] photoluminescence (PL),[13–16] humidity sensor[17–19] and magnetic properties[20,21] as well as electronic properties for the tungstates.

Among these tungstates, the investigation of iron tungstate ($FeWO_4$) has been widely reported in the literature due to good magnetic,[22,23] and photocatalytic[24,25] properties. Therefore, Zhang *et al.*[26] have developed a new synthesis method to obtain different $FeWO_4$ meso-, micro- and nanocrystals with superior electronic properties. Several synthesis methods are used in the preparation of $FeWO_4$ nanocrystals, but the conventional hydrothermal (CH) method has most often been employed and reported in the literature.[27–30] However, the CH method has some inconveniences, such as a long time period (typically one-half to several days) because of slow heat transfer due to the conduction and convection transport mechanism and high electric power usage (over a thousand watts). The solution to these problems is the microwave-hydrothermal (MH) method; this method facilitates the attainment of this oxide material in a shorter time and with lower energy consumption[31] which is possible due to efficient internal heating (in-core volumetric heating) by direct coupling of microwave irradiation with solvent molecules, ions and hydroxides in the reaction mixture.[32]

Therefore, in this communication, we have employed the MH method for the fast preparation of $FeWO_4$ nanocrystals with different orientations by the use of surfactants. Moreover, we have analyzed their structure, size, shape, and PL properties at room temperature.

2. Experimental procedure

2.1. Microwave-hydrothermal synthesis of $FeWO_4$ nanocrystals

A typical synthesis of $FeWO_4$ nanocrystals was conducted as follows: 1×10^{-3} mol of sodium tungstate (VI) dihydrate ($Na_2WO_4 \cdot 2H_2O$) (99.5% purity, Sigma-Aldrich) and 1×10^{-3} mol of ammoniacal ferrous sulfate ($[(NH_4)_2Fe(SO_4)_2 \cdot 6H_2O]$)

[a]*LIEC, Department of Chemistry, Federal University of São Carlos, C. Postal 676, Rod. Washington Luis, Km 235, 13565-905, São Carlos, SP, Brazil. E-mail: laeciosc@bol.com.br*
[b]*INCTMN, Institute of Chemistry, Unesp, Araraquara, SP, 14800-900, Brazil*
[c]*MAv -DF-Universidade Estadual, Paulista, C. Postal 473, Bauru, SP, 17033-360, Brazil*
[d]*IFSC-Universidade de São Paulo, São Carlos, SP, 13560-970, Brazil*
[e]*Thin Films & Nanomaterials Laboratory, Department of Physics, Bharathiar University, Coimbatore, 641 046, India*
† Electronic supplementary information (ESI) available. See DOI: 10.1039/c2ce25771h

(99% purity, Sigma-Aldrich) were dissolved in 100 mL of water (pH = 9). In separate experiments, the following quantities of surfactants were dissolved in enough ionized water to produce 100 mL of solution; a) 0.04 mol of dioctyl sodium sulfosuccinate ($C_{20}H_{37}NaO_7S$) (99% purity, Sigma-Aldrich), abbreviated as AOT; b) 50 mL of polyethylene glycol ($C_{2n}H_{4n+2}O_{n+1}$) (99% purity, Sigma-Aldrich) with a molecular mass (MW = 200), abbreviated as PEG-200. These solutions were added separately to the tungstate/iron solution, and the mixtures were placed in a Teflon autoclave which was sealed and placed inside a domestic MH system at 170 °C for 45 min. The resulting suspensions were washed with deionized water and acetone to remove residual Na^+ ions. Finally, crystalline $FeWO_4$ nanocrystals (black color) were collected on a filter and dried with acetone at room temperature for several hours.

2.2. Characterizations

These $FeWO_4$ nanocrystals were structurally characterized by X-ray diffraction (XRD) patterns using a D/Max-2500PC diffractometer (Rigaku, Japan) with Cu-Kα radiation (λ = 1.5406 Å) in the 2θ range from 10 to 60° and from 10 to 110° both with a scanning velocity of 1° min^{-1} in the Rietveld routine (8 h of measurement). The shape and size of these $FeWO_4$ nanocrystals were observed by transmission electron microscopy (TEM) and high resolution TEM (HR-TEM) using a TECNAI F20 FEI microscopy operated at 200 kV. PL measurements were taken with a Monospec 27 monochromator (Thermal Jarrel Ash, USA) coupled to a R446 photomultiplier (Hamamatsu Photonics, Japan). A krypton ion laser (Coherent Innova 90 K, USA) (λ = 350 nm) was used as the excitation source; the maximum output power was maintained at 500 mW. The laser beam was passed through an optical chopper; the maximum power on the sample was maintained at 40 mW. PL measurements were taken at room temperature.

3. Results and discussion

3.1. XRD patterns and Rietveld refinement analyses of $FeWO_4$ crystals

Fig. 1 shows XRD patterns for $FeWO_4$ nanocrystals prepared by the MH method at 170 °C for 45 min: (a) without surfactant, (b) AOT anionic surfactant and (c) PEG-200 non-ionic surfactant.

XRD patterns in Fig. 1(a–c) indicate that $FeWO_4$ nanocrystals have a wolframite-type monoclinic structure with a space group of ($P2/c$) and a point group symmetry (C_{2h}^4) as described in the respective Joint Committee on Powder Diffraction Standards (JCPDS) card No. 46-1446.[33] These crystals have a broad diffraction peak which indicates possibly the presence of nanocrystals with a reasonable degree of structural order and crystallinity at long range. Moreover, Fig. 1(c) demonstrates that $FeWO_4$ nanocrystals prepared with PEG-200 (non-ionic surfactant) exhibited a partial effect of crystallographic orientation in relation to other $FeWO_4$ nanocrystals (see Fig. 1 (a–c)). Diffraction peaks associated with the (011)/(110) plane clearly verify this phenomenon, especially when compared to the standard diffraction pattern (JCPDS card No. 46-1446)[33] and with the other nanocrystals. Based on this information, it was observed that

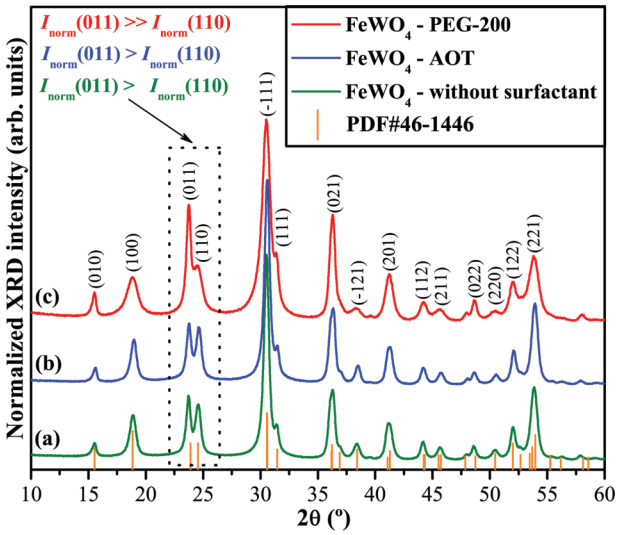

Fig. 1 Normalized XRD patterns of $FeWO_4$ nanocrystals synthesized by the MH method at 170 °C for 45 min: (a) without surfactant, (b) AOT anionic surfactant and (c) PEG-200 non-ionic surfactant. The vertical lines indicate the position and relative intensity of the JCPDS card No. 46-1446 for the $FeWO_4$ phase.

$I_{norm}(011) > I_{norm}(110)$ (see Fig. 1(a)); $I_{norm}(011) > I_{norm}(110)$ (see Fig. 1(b)); and $I_{norm}(011) \gg I_{norm}(110)$ (see Fig. 1(c) for $FeWO_4$ without surfactant, with AOT anionic surfactant and with PEG-200, respectively.

Fig. 2(a–c) show the Rietveld refinement plot for $FeWO_4$ nanocrystals prepared by the MH method at 170 °C for 45 min: (a) without surfactant, (b) AOT anionic surfactant and (c) PEG-200 non-ionic surfactant, respectively.

The structural refinement using the Rietveld method[34] was performed to confirm the monoclinic structure for $FeWO_4$ nanocrystals.[35] Therefore, the structural refinement method was employed in this work because it has several advantages over conventional quantitative analysis methods. This method uses a whole pattern-fitting algorithm where all lines for each phase are explicitly considered, and even severely overlapped lines are usually not a problem.[36]

The structural refinement was performed using the GSAS software[37] which revealed the Rietveld texture and stress analysis.[38] The quality of structural refinement is generally checked by R-values (R_{wp}, R_{bragg}, χ^2, and S), and these numbers are easy to detect as they are consistent with a monoclinic structure. However, a difference in plotting observed and calculated patterns is the best way to judge the success of Rietveld refinement.[39] Moreover, other parameters with additional functions were applied to find a structural refinement with better quality and reliability. The optimized parameters were: scale factor, background with exponential shift, exponential thermal shift and polynomial coefficients, basic phase, microstructure, crystal structure, size strain (anisotropic, no rules), structure solution model (genetic algorithm SDPD), shift lattice constants, profile half-width parameters (u, v, w), texture, lattice parameters (a, b, c), factor occupancies and atomic site occupancies (Wyckoff). The Rietveld refinement was performed based on the α-$FeWO_4$ phase with a monoclinic structure using a better approximation and indexing of the Crystallographic Information File (CIF) and employing CIF

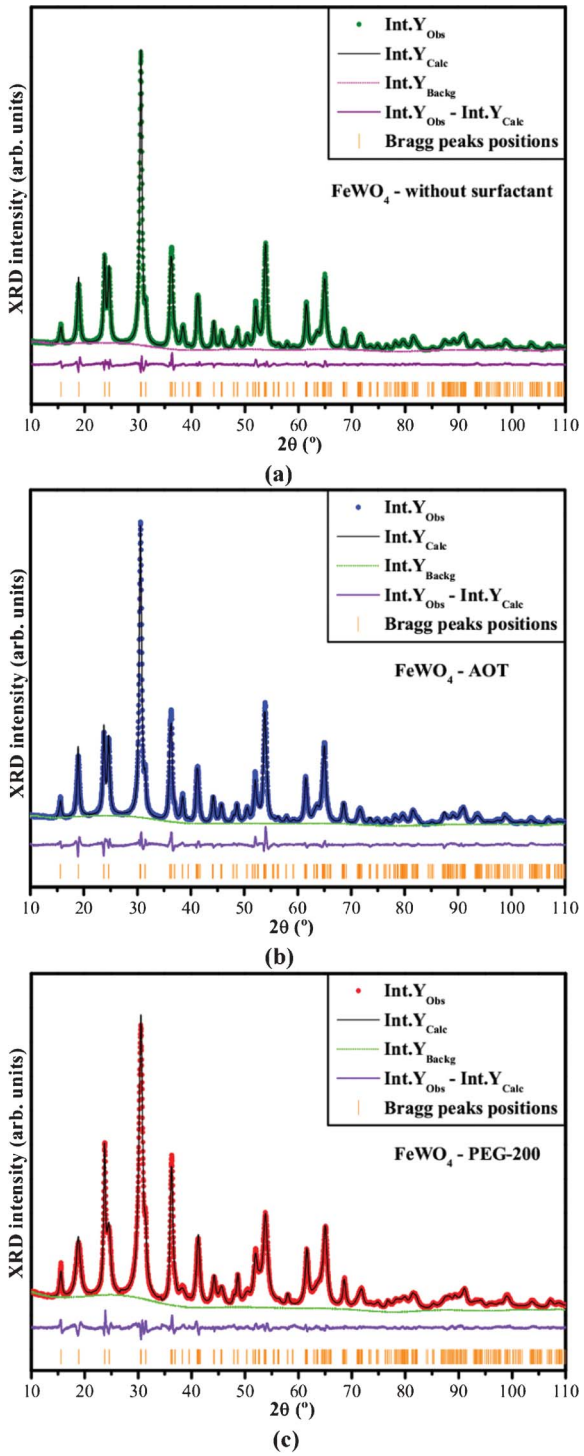

Fig. 2 Rietveld refinement plot of $FeWO_4$ nanocrystals synthesized by the MH method at 170 °C for 45 min: (a) without surfactant, (b) AOT anionic surfactant and (c) PEG-200 non-ionic surfactant.

No. 26843.[40] Therefore, Fig. 2(a–c) illustrate good agreement between the experimentally observed XRD patterns and theoretically fitted results, which indicate the success of the Rietveld refinement method (see Table 1).

In this table, the fit parameters (R_{wp}, R_{bragg}, χ^2, and S) suggest that refinement results are very reliable. We have observed some small variations in the atomic positions related to the oxygen atoms while the iron and tungsten atoms retain their fixed positions within the structure. These results indicate major structural distortions on [FeO_6] and [WO_6] clusters of $FeWO_4$ nanocrystals prepared with the PEG-200 (polymer surfactant) which can be due to the partial effect of crystallographic orientation in the (011) plane.

Table 1 Lattice parameters, unit cell volume, atomic coordinates and site occupation obtained by Rietveld refinement data for the $FeWO_4$ nanocrystals prepared by the MH at 170 °C for 45 min: without surfactant, OAT anionic surfactant, and PEG-200 non-ionic surfactant

Atoms[a]	Wyckoff	Site	*x*	*y*	*z*
Fe	2*f*	2	0.5000	0.6674	0.2500
W	2*e*	2	0.0000	0.1746	0.2500
O1	4*g*	1	0.2260	0.1148	0.5542
O2	4*g*	1	0.2618	0.3715	0.1068

[a] $FeWO_4$ – without surfactant. *P*2/*c* (13) - monoclinic, a = 4.692(3) Å, b = 5.695(5) Å, c = 4.979(6) Å; V = 133.08 Å^3; $\alpha = \gamma = 90°$, β = 89.95°; R_{wp} = 4.81%; R_{bragg} = 1.74% , χ^2 = 4.14 and S = 2.034.

Atoms[b]	Wyckoff	Site	*x*	*y*	*z*
Fe	2*f*	2	0.5000	0.6704	0.2500
W	2*e*	2	0.0000	0.1727	0.2500
O1	4*g*	1	0.2374	0.1238	0.5412
O2	4*g*	1	0.2474	0.3732	0.1174

[b] $FeWO_4$ – AOT. *P*2/*c* (13) - monoclinic, a = 4.684(3) Å, b = 5.694(3) Å, c = 4.982(1) Å; V = 132.89 Å^3; $\alpha = \gamma = 90°$, β = 89.96°; R_{wp} = 5.98%; R_{bragg} = 4.21% , χ^2 = 6.65 and S = 2.578.

Atoms[c]	Wyckoff	Site	*x*	*y*	*z*
Fe	2*f*	2	0.5000	0.6675	0.2500
W	2*e*	2	0.0000	0.1759	0.2500
O1	4*g*	1	0.2392	0.1093	0.5423
O2	4*g*	1	0.2274	0.3575	0.1479

[c] $FeWO_4$ – PEG-200. *P*2/*c* (13) - monoclinic, a = 4.703(3) Å, b = 5.696(5) Å, c = 4.971(1) Å; V = 133.19 Å^3; $\alpha = \gamma = 90°$, β = 89.83°; R_{wp} = 4.87%; R_{bragg} = 3.87% , χ^2 = 4.83 and S = 2.197.

3.2. Representation of $FeWO_4$ unit cells

Fig. 3(a–c) illustrate a schematic representation for monoclinic $FeWO_4$ unit cells modeled from Rietveld refinement data for $FeWO_4$ nanocrystals prepared by the MH method at 170 °C for 45 min: (a) without surfactant, (b) AOT anionic surfactant and (c) PEG-200 non-ionic surfactant, respectively.

These unit cells were modeled through the Visualization for Electronic and Structural Analysis (VESTA) software version 3.1.1 for Windows[41] using lattice parameters and atomic positions obtained from Rietveld refinement data shown in Table 1. $FeWO_4$ crystals belong to a wolframite-type monoclinic structure with a space group of (*P*2/*c*), a point-group symmetry (C_{2h}^4) and two formulae per unit cell (Z = 2)[42] Fig. 3(a–c) verifies that bonds between O–Fe–O and O–W–O atoms were projected out of unit

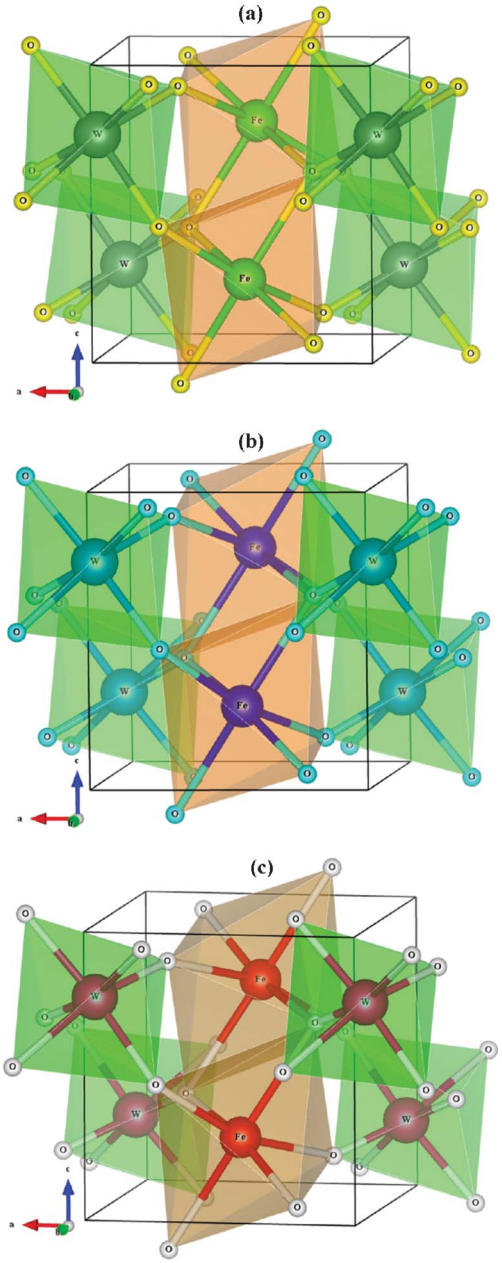

Fig. 3 Schematic representations of crystalline unit cells of $FeWO_4$ nanocrystals obtained at 170 °C for 45 min: (a) without surfactant, (b) AOT anionic surfactant, and (c) PEG-200 non-ionic surfactant.

cells. In these unit cells, all tungsten (W) and iron (Fe) atoms are coordinated only to six four-oxygen atoms which form distorted $[FeO_6]/[WO_6]$ clusters with a octahedral configuration, a symmetry group (O_h) and octahedral polyhedra (6 vertices, 8 faces and 12 edges).[43] Moreover, a reasonable level of distortion on $[FeO_6]/[WO_6]$ clusters in the lattice of $FeWO_4$ crystals prepared with PEG-200 can be verified. These differences in (O–Fe–O)/(O–W–O) bond angles can produce different levels of order–disorder and/or distortions in the $FeWO_4$ crystal lattice.

3.3. TEM, HR-TEM and SAED analyses of $FeWO_4$ nanocrystals

Fig. 4(a–f) show TEM/HR-TEM images and selected area electron diffraction (SAED) patterns for $FeWO_4$ nanocrystals obtained at 170 °C for 45 min: (a,b) without surfactant, (c,d) AOT anionic surfactant and (e,f) PEG-200 non-ionic surfactant, respectively.

The TEM image in Fig. 4(a) illustrates several rods-like $FeWO_4$ nanocrystals with an agglomerate nature as well as polydisperse shapes in a size distribution. These images also indicate that these nanocrystals are formed and grow quickly in an aqueous solution after microwave irradiation, which promotes a fast precipitation reaction.[44] The inset in Fig. 4(a) shows that SAED patterns exhibited rings that are characteristic for rod-like $FeWO_4$ nanocrystals. The HR-TEM image in Fig. 4(b) reveals two nanoparticles in the oriented attachment growth process that results in a nanorod. These nanocrystals have an anisotropic preferential growth along the [100] direction, which is in agreement with recent work reported in the literature for wolframite-type nanocrystals.[45] The type of growth occurs due to differences in surface energies on each nanocrystal face. Moreover, the HR-TEM image in the inset in Fig. 4(b) displays some nanorods oriented in the same (001) plane (with an interplanar spacing of approximately 4.96 Å). From the counts of several nanorods, the $FeWO_4$ synthesized in water shows an average rod size of 25.5 nm. Fig. 4(c) shows the effect of AOT surfactant on the growth of aggregated larger rods. Moreover, the inset in Fig. 4(c) exhibits some single $FeWO_4$ nanorods. From the counts of several nanorods, the average rod size was 32.5 nm. HR-TEM images in Fig. 4(d) reveals that some of these nanorods aggregated in the same (100) plane. As a result of the oriented attachment (OA) nanoparticles grow in the [100] direction by sharing the sample crystal facet.[46] The inset in Fig. 4(d) illustrates FFT patterns typical of $FeWO_4$ single crystal; *i.e.*, a well formed crystal followed by an OA growth process which results in rod-like-shaped nanocrystals. Fig. 4(e) shows the TEM image of several anisotropic rod-like $FeWO_4$ aggregated nanocrystals prepared with PEG-200 surfactant. The counts of several nanorods reveal the growth of rods with an average size of 23.5 nm. The SAED in the inset shows the indexed polycrystalline monoclinic structure (inset of Fig. 4(f)). In addition, Fig. 4(f) illustrates the HR-TEM image of two $FeWO_4$ nanorods with crystallographic fusion in the same (100) plane. These two nanocrystals have a specific crystallographic relationship (coincident site lattice matching) where these nanorods adhere strongly and fuse to form a large crystal.[47] In fact, as evidence in the XRD patterns the $FeWO_4$ nanocrystals prepared with PEG-200 have been showed a partial preferential orientation in the (011) direction. Then a fraction of the nanoparticles exhibit a preferential orientation in this direction. However, it is not possible to observe this effect in our HR-TEM images (Fig. 4f) due to the attachment oriented occurs in a plane different. Therefore, it is possible to infer that this behavior has a relationship with force bonds (O–Fe–O)/(O–W–O), fusion between the crystallographic plane with low surface energy and distorted octahedrons on $[FeO_6]$ and $[WO_6]$ clusters that induces an orientation in different crystallographic planes with high surface energy and effective electronic activity. However, future calculations will be performed to understand the influence of surface energies on the crystal growth process of $FeWO_4$ nanocrystals. Moreover, Fig. 4(f) shows the HR-TEM image of two nanorods in the process of self-assembly by mean of an OA mechanism which occurs with a self-assembly by sharing a common crystallographic orientation and the docking of these nanocrystals at a planar interface.[48] The results indicate that these rod-like $FeWO_4$

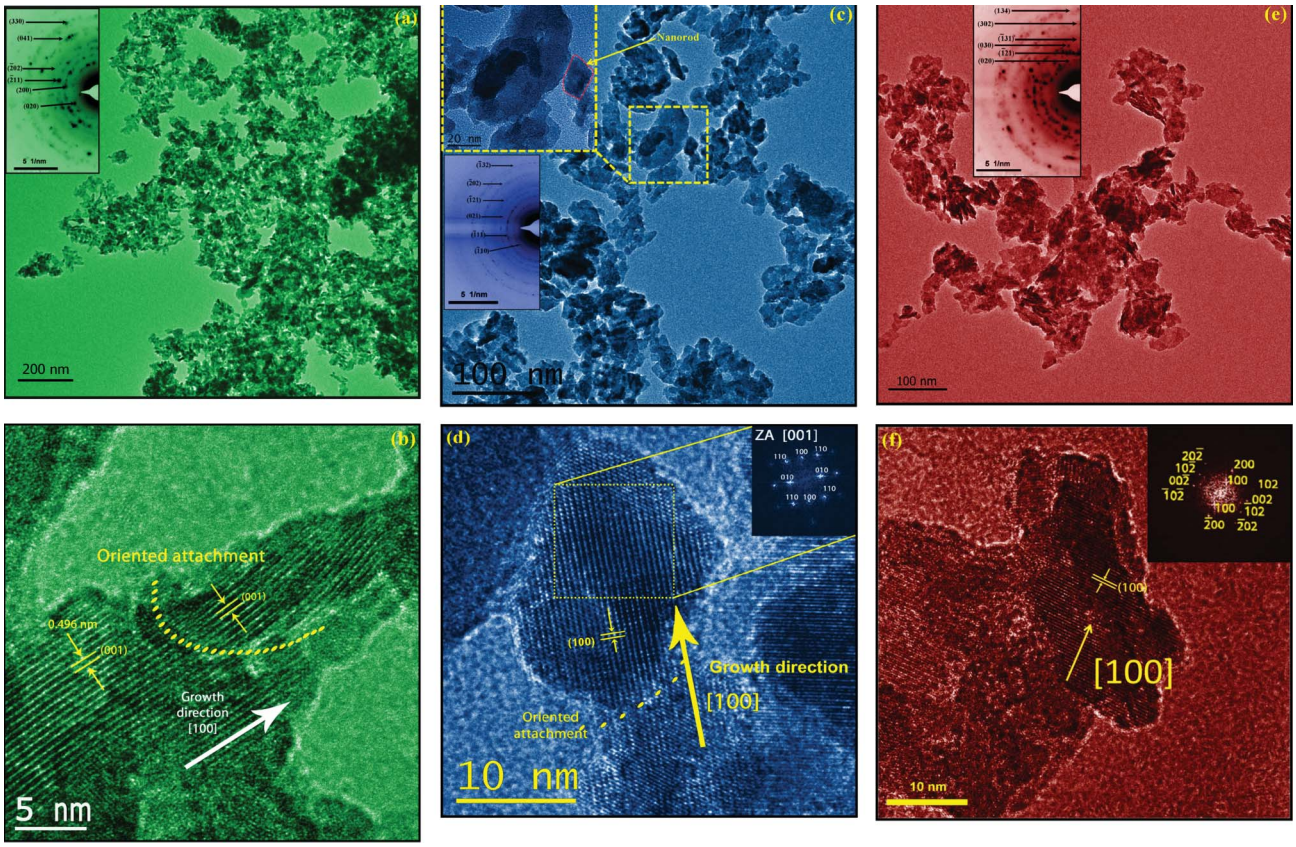

Fig. 4 TEM/HR-TEM image and SAED patterns of $FeWO_4$ nanocrystals synthesized by the MH method at 170 °C for 45 min: (a,b) without surfactant, (c,d) AOT anionic surfactant and (e,f) PEG-200 non-ionic surfactant.

nanocrystals prepared with PEG-200 surfactant grew in a partial preferential orientation (XRD patterns, Fig. 1(a–c)), which is different from $FeWO_4$ nanocrystals prepared without surfactant and an AOT anionic surfactant. SAED pattern analyses indicate that $FeWO_4$ nanocrystals prepared with PEG-200 surfactant have a high crystallinity in relation to other nanocrystals. Moreover, HR-TEM images verified that the surfaces of the nanocrystals are well defined when compared to $FeWO_4$ nanocrystals prepared without and with AOT surfactant, which can exhibit a partly amorphous surface (see ESI, Fig. SI†).

3.4. PL properties of $FeWO_4$ microcrystals

Fig. 5 illustrates the PL spectra at room temperature of $FeWO_4$ nanocrystals prepared by the MH method at 170 °C for 45 min: (a) without surfactant, (b) AOT anionic surfactant and (c) PEG-200 non-ionic surfactant.

According to research reported in the literature,[49,50] blue PL properties of $FeWO_4$ crystals are related to the radiative recombination of self-trapped excitons localized on a regular WO_4^{2-} complex anion, whereas green PL properties are extrinsic and may be a defect-related emission. However, all these phenomena are directly associated with WO_4^{2-} groups (ions), which appear only in an aqueous solution since $FeWO_4$ crystals are crystalline solids composed of interconnected clusters (⋯[WO_6]–[FeO_6]–[WO_6]⋯), as shown in Fig. 5(a–c). Therefore, in this communication, we assume that PL properties of $FeWO_4$ crystals are due to different types of electronic transitions between

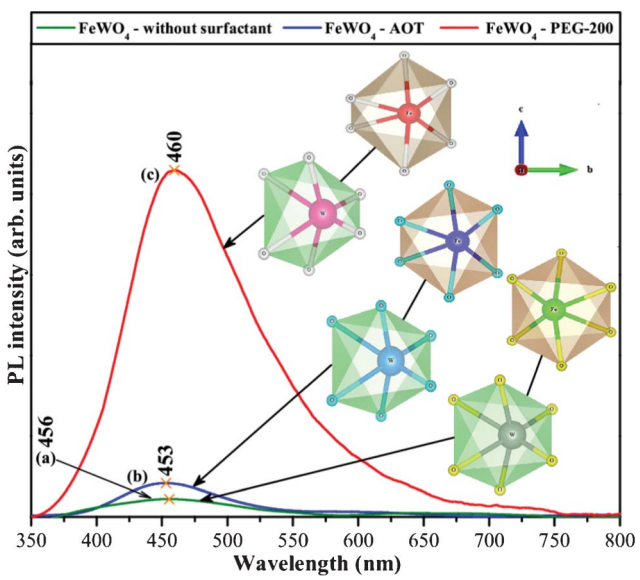

Fig. 5 PL spectra of rod-like $FeWO_4$ nanocrystals synthesized by the MH method at 170 °C for 45 min: (a) without surfactant, (b) AOT anionic surfactant and (c) PEG-200 non-ionic surfactant. Insets show distortions on octahedral [FeO_6]/[WO_6] clusters modeled from Rietveld refinement data.

the valence band and the conduction band. Therefore, we have observed different optical band gap values. These electronic defects were provoked by the distortion in octahedral $[FeO_6]/[WO_6]$ clusters in the lattice (see inset in Fig. 5(a–c)). Moreover, Fig. 5(c) confirms that the PEG-200 surfactant was responsible for improvement in PL properties. This behavior is related to the partial effect of crystallographic orientation in the (011) plane which causes different distortions in octahedral $[FeO_6]/[WO_6]$ clusters. As reported in the literature,[49,50] the PL intensity enhancement may be due to the shape of the products and the improved crystallinity. Experimental results obtained by Zhang *et al.*[50] indicate that luminescence properties of $FeWO_4$ are very sensitive to their morphology and strongly dependent on the size. However, in this present communication, we discovered a new factor that affects the intensity of PL emission of $FeWO_4$ nanocrystals: the effect of changes in the partial crystallographic orientation and distortions in octahedral $[FeO_6]/[WO_6]$ clusters.

4. Conclusions

In summary, we have obtained with success rod-like $FeWO_4$ nanocrystals by the MH method at 170 °C for 45 min. XRD patterns and Rietveld refinement data indicate that these crystals are monophasic with a monoclinic structure. Structural refinement data were employed to model distorted octahedral $[FeO_6]/[WO_6]$ clusters in the lattice of $FeWO_4$ nanocrystals. TEM and HR-TEM images show that nanocrystals grow by self-assembly, an oriented attachment process and the aggregation of small nanocrystals with a further growth of rod-like $FeWO_4$ crystals. Moreover, an effect of oriented growth was verified for $FeWO_4$ nanocrystals prepared with PEG-200. Finally, we have observed that PL properties of these nanocrystals are dependent on distortions in octahedral $[FeO_6]/[WO_6]$ clusters and partial preferential orientation in the (011) crystallographic plane of these nanocrystals.

Acknowledgements

The authors are grateful for the financial support from Brazilian research financing institutions: FAPESP (No. 2009/53189-8 and 2009/50303-4), CNPq (159710/2011-1) and CAPES.

References

1 S. Song, Y. Zhang, J. Feng, X. Ge, D. Liu, W. Fan, Y. Lei, Y. Xing and H. Zhang, *CrystEngComm*, 2009, **11**, 1987.
2 T. D. Nguyen, D. Mrabet, T. T. D. Vu, C. T. Dinh and T. O. Do, *CrystEngComm*, 2011, **13**, 1450.
3 Y. Li, S. Tan, J. Jiang, Z. Huang and X. Tan, *CrystEngComm*, 2011, **13**, 2649.
4 S. H. Yu, M. Antonietti, H. Cölfen and M. Giersig, *Angew. Chem.*, 2002, **114**, 2462.
5 X. He, M. Guan, Z. Li, T. Shang, N. Lian and Q. Zhou, *J. Am. Ceram. Soc.*, 2011, **94**, 2483.
6 J. Liao, B. Qiu, H. R. Wen, Y. Li, R. Hong and H. You, *J. Mater. Sci.*, 2011, **46**, 1184.
7 L. Gracia, V. M. Longo, L. S. Cavalcante, A. Beltrán, W. Avansi, M. S. Li, V. R. Mastelaro, J. A. Varela, E. Longo and J. Andrés, *J. Appl. Phys.*, 2011, **110**, 043501.
8 L. S. Cavalcante, V. M. Longo, J. C. Sczancoski, M. A. P. Almeida, A. A. Batista, J. A. Varela, M. O. Orlandi, E. Longo and M. Siu Li, *CrystEngComm*, 2012, **14**, 853.
9 A. Kalinko and A. Kuzmin, *J. Non-Cryst. Solids*, 2011, **357**, 2595.
10 M. A. P. Almeida, L. S. Cavalcante, M. S. Li, J. A. Varela and E. Longo, *J. Inorg. Organomet. Polym. Mater.*, 2012, **22**, 264.
11 L. Gigorjeva, D. Millers, J. Grabis and D. Jankoviča, *Cent. Eur. J. Phys.*, 2011, **9**, 510.
12 H. Fu, C. Pan, L. Zhang and Y. Zhu, *Mater. Res. Bull.*, 2007, **42**, 696.
13 B. S. Barros, A. C. de Lima, Z. R. da Silva, D. M. A. Melo and S. Alves-Jr, *J. Phys. Chem. Solids*, 2012, **73**, 635.
14 J. Liao, L. Liu, H. You, H. Huang and W. You, *Optik*, 2012, **123**, 901.
15 Y. F. Liu, S. H. Dai, Y. N. Lu and H. H. Min, *Powder Technol.*, 2012, **221**, 412.
16 W. L. Feng, M. F. Zhao, J. Y. Xue and X. J. Tian, *J. Alloys Compd.*, 2012, **521**, 146.
17 W. Qu, W. Wlodarski and J. U. Meyer, *Sens. Actuators, B*, 2000, **64**, 76.
18 L. You, Y. Cao, Y. F. Sun, P. Sun, T. Zhang, Y. Du and G. Y. Lu, *Sens. Actuators, B*, 2012, **161**, 799.
19 N. Ichinose, *Sens. Actuators, B*, 2012, **13**, 100.
20 M. Maczka, M. Ptak, A. Pikul, L. Kepinski, P. E. Tomaszewski and J. Hanuza, *Vibrat. Spectr.*, 2012, **58**, 163.
21 F. Ye, Y. Ren, J. A. Fernandez-Baca, H. A. Mook, J. W. Lynn, R. P. Chaudhury, Y. Q. Wang, B. Lorenz and C. W. Chu, *Phys. Rev. B.*, 2008, **78**, 193101.
22 H. A. Obermayer, H. Dachs and H. Schrocke, *Solid State Commun.*, 1973, **12**, 779.
23 F. Wegner, *Solid State Commun.*, 1973, **12**, 785.
24 Y. X. Zhou, H. B. Yao, Q. Zhang, J. Y. Gong, S. J. Liu and S. H. Yu, *Inorg. Chem.*, 2009, **48**, 1082.
25 H. H. A. Ghafar, M. Inagaki, T. Tsumura and M. Toyoda, *The Open Materials Science Journal*, 2008, **2**, 56.
26 J. Zhang, Y. Zhang, J. Y. Yan, S. K. Li, H. S. Wang, F. Z. Huang, Y. H. Shen and A. J. Xie, *J. Nanopart. Res.*, 2012, **14**, 796.
27 S. Rajagopal, V. L. Bekenev, D. Nataraj, D. Mangalaraj and O. Khyzhun, *J. Alloys Compd.*, 2010, **496**, 61.
28 S. Rajagopal, D. Nataraj, O. Y. Khyzhun, Y. Djaoued, J. Robichaud and D. Mangalaraj, *J. Alloys Compd.*, 2010, **493**, 340.
29 H. W. Shim, I. S. Cho, K. S. Hong, W. I. Cho and D. W. Kim, *Nanotechnology*, 2010, **21**, 465602.
30 S. H. Yu, B. Liu, M. S. Mo, J. H. Huang, X. M. Liu and Y. T. Qian, *Adv. Funct. Mater.*, 2003, **13**, 639.
31 D. P. Volanti, M. O. Orlandi, J. Andrés and E. Longo, *CrystEngComm*, 2010, **12**, 1696.
32 M. Baghbanzadeh, L. Carbone, P. D. Cozzoli and C. O. Kappe, *Angew. Chem., Int. Ed.*, 2011, **50**, 11312.
33 A. Sugaki, A. Kitakaze and K. Hayashi, *Sci. Reports Tohoku University*, 1986, **16**, 353.
34 H. M. Rietveld, *J. Appl. Crystallogr.*, 1969, **2**, 65.
35 A. P. Young and C. M. Schwartz, *Science*, 1963, **141**, 348.
36 J. M. Amigó, J. V. Clausell, V. Esteve, J. M. Delgado, M. M. Reventos, L. E. Ochando, T. Debaerdemaeker and F. Marti, *J. Eur. Ceram. Soc.*, 2004, **24**, 75.
37 A. C. Larson and R. B. Von Dreele, *General Structure Analysis System (GSAS), Los Alamos National Laboratory Report LAUR*, 1994, 86–748.
38 B. H. Toby, *J. Appl. Crystallogr.*, 2001, **34**, 210.
39 G. Will, *Powder diffraction: The Rietveld method and the two stage method to determine and refine crystal structures from powder diffraction data*, Springer-Verlag Berlin Heidelberg, 2006, pp. 44–69.
40 D. Ulku, *Z. Kristallogr.*, 1967, **124**, S192.
41 K. Momma and F. Izumi, *J. Appl. Crystallogr.*, 2011, **44**, 1272.
42 J. Ruiz-Fuertes, S. López-Moreno, D. Errandonea, J. Pellicer-Porres, R. Lacomba-Perales, A. Segura, P. Rodríguez-Hernández, A. Muñoz, A. H. Romero and J. González, *J. Appl. Phys.*, 2010, **107**, 083506.
43 http://en.wikipedia.org/wiki/Octahedron, accessed 1st August 2012.
44 M. A. P. Almeida, L. S. Cavalcante, J. A. Varela, M. S. Li and E. Longo, *Adv. Powder Technol.*, 2012, **23**, 124.
45 H. W. Shim, A. H. Lim, G. H. Lee, H. C. Jung and D. W. Kim, *Nanoscale Res. Lett.*, 2012, **7**, 9.
46 P. Li, X. Zhao, Y. Li, H. Sun, L. Sun, X. Cheng, X. Hao and W. Fan, *CrystEngComm*, 2012, **14**, 920.
47 L. S. Cavalcante, J. C. Sczancoski, R. L. Tranquilin, J. A. Varela, E. Longo and M. O. Orlandi, *Particuology*, 2009, **7**, 353.
48 J. C. Sczancoski, M. D. R. Bomio, L. S. Cavalcante, M. R. Joya, P. S. Pizani, J. A. Varela, E. Longo, M. S. Li and J. A. Andrés, *J. Phys. Chem. C*, 2009, **113**, 5812.
49 W. Hu, Y. Zhao, Z. Liu, C. W. Dunnill, D. H. Gregory and Y. Zhu, *Chem. Mater.*, 2008, **20**, 5657.
50 J. Zhang, Y. Wang, S. Li, X. Wang, F. Huang, A. Xie and Y. Shen, *CrystEngComm*, 2011, **13**, 5744.

